Spectroelectrochemical Evaluation of Redox Potentials of Cysteine Tryptophylquinone and Two Hemes *c* in Quinohemoprotein Amine Dehydrogenase from *Paracoccus denitrificans*†

Nobutaka Fujieda, Megumi Mori, Kenji Kano,* and Tokuji Ikeda

Division of Applied Life Sciences, Graduate School of Agriculture, Kyoto University, Sakyo-ku, Kyoto 606-8502, Japan

Received July 9, 2002; Revised Manuscript Received September 3, 2002

ABSTRACT: Quinohemoprotein amine dehydrogenase (QH-AmDH) from *Paracoccus denitrificans* has a novel cofactor cysteine tryptophylquinone (CTQ) in the smallest γ subunit and two hemes *c* in the largest α subunit [Datta, S., Mori, Y., Takagi, K., Kawaguchi, K., Chen, Z., Okajima, T., Kuroda, S., Ikeda, T., Kano, K., Tanizawa, K., and Mathews, F. S. (2001) *Proc. Natl. Acad. Sci. U.S.A. 98,* 14268−14273]. The spectral change of QH-AmDH was assigned to the redox reaction of the hemes *c* alone. The redox potentials of the two hemes *c* with His and Met as the second axial ligands, respectively, were determined to be 0.149 and 0.235 V versus SHE at pH 7.0 by a mediator-assisted continuous-flow column electrolytic spectroelectrochemistry (MCES). The monomeric γ subunit of QH-AmDH was isolated from urea-treated QH-AmDH. The fully oxidized and reduced forms of the γ subunit exhibited a unique absorption band centered at 380 nm and a shoulder band around 315 nm, respectively, at neutral pH. The two-electron redox potential of CTQ in the isolated γ subunit was evaluated to be 65 mV at pH 7.0 by MCES. The redox reaction was linked to the two-proton transfer at pH <8.6 and to a single-proton transfer at pH >8.6. The pK_a value (K_a being the acid dissociation constant) of 8.6 was assigned to one of the phenolic OH groups of the quinol form. Upon deprotonation, the red shift of the shoulder band was observed. The γ subunit adsorbed on a glassy carbon electrode, and gave a direct but quasi-reversible electrochemical signal. Intra- and interprotein electron transfers of QH-AmDH are discussed from thermodynamic and structural points of view.

Quinoprotein amine dehydrogenases are induced when several methylotrophic bacteria are grown on media that include biological amines as the sole source of carbon, nitrogen, and energy (*1*). *Paracoccus denitrificans* IFO 12442 expresses two types of amine dehydrogenases, methylamine dehydrogenase (MADH)[1] (*2*) and quinohemoprotein amine dehydrogenase (QH-AmDH) (*3*), when grown on methylamine and longer chain amines such as *n*-butylamine, respectively. Both enzymes catalyze the oxidation of the primary amines to yield the corresponding aldehyde and ammonia. Aromatic amine dehydrogenase (*4*, *5*) and quinohemoprotein amine dehydrogenase (*6*, *7*), which are structurally very close to MADH and QH-AmDH from *P. denitrificans*, respectively, are expressed in *Alcaligenes faecalis* and *Pseudomonas putida*, respectively.

MADH has an $\alpha_2\beta_2$ quaternary structure, and contains a covalently bound posttranslationally generated quinone cofactor, tryptophan tryptophylquinone (TTQ), on each of the smaller β subunits as the catalytic center, while the larger α subunit does not possess any prosthetic group (*8*). The physiological electron acceptor of MADH is amicyanin, a typical type I copper protein (*9*). Amicyanin is induced together with MADH because the genes encoding these proteins are built in one operon, the *mau* gene cluster (*10*). The kinetics of electron transfer from the MADH to amicyanin have been documented (*11*). The redox potential, $E^{\circ\prime}$, has been reported to be 0.100 (*12*) or 0.130 V (*13*) for MADH from *P. denitrificans*, and 0.093 V for MADH from bacterium W3A1 (*14*). The crystallographic structure of the MADH−amicyanin complex has been determined and shows that hydrophobic residues play an important role in the interaction (*15*). Kinetic and thermodynamic studies coupled with site-directed mutagenesis have revealed the importance of ionic interactions as well as hydrophobic interactions (*16*−*18*).

On the other hand, the crystallographic structure of QH-AmDH from *P. denitrificans* and *Ps. putida* has recently been revealed by two groups (*19*, *20*). QH-AmDH is an $\alpha\beta\gamma$ heterotrimeric protein (Figure 1). The smallest γ subunit has a novel quinone cofactor, cysteine tryptophylquinone (CTQ) (Figure 2), which is formed by posttranslational modification of residues Cys37γ and Trp43γ. The largest α subunit has two heme *c* groups. One of the hemes *c* [called heme *c*(a)] is solvent accessible and has His and Met as the first and second axial ligands, respectively, as in the case of the usual cytochrome *c* (*21*). The other one [called heme *c*(b)] is buried almost fully and located between CTQ and heme *c*(a). Heme *c*(b) has bisaxial His ligands, as in the case of cytochrome

† This work was financially supported in part by Grants-in-Aid for Scientific Research from the Ministry of Education, Science, Sports and Culture of Japan to K.K. and T.I.

* To whom correspondence should be addressed. Fax: +81-75-753-6456. E-mail: kkano@kais.kyoto-u.ac.jp.

[1] Abbreviations: MADH, methylamine dehydrogenase; QH-AmDH, quinohemoprotein amine dehydrogenase; TTQ, tryptophan tryptophylquinone; CTQ, cysteine tryptophylquinone; MCES, mediator-assisted continuous-flow column electrolytic spectroelectrochemistry.

10.1021/bi026387v CCC: $22.00
Published on Web 10/22/2002

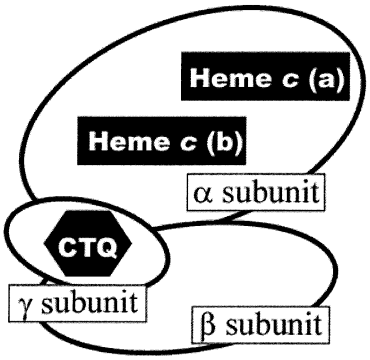

FIGURE 1: Schematic picture of the subunit structure of QH-AmDH.

c_3 (*22*). In this respect, the diheme-containing domain in the α subunit is similar to diheme cytochrome *c* peroxidase (*23*). Another novel feature of QH-AmDH is that all cysteine residues in the γ subunit are in thioether linkages with Asp or Gln (*19*, *20*). The electron acceptor of QH-AmDH has been found to be cytochrome c_{550} in *P. denitrificans* (*24*) but azurin in *Ps. putida* (*7*).

For further understanding of the intramolecular electron transfer of QH-AmDH, it is very important to determine $E^{\circ\prime}$ values of all three redox centers in the enzyme (*25*). In a previous paper, our group tried to evaluate the $E^{\circ\prime}$ values of the heme and quinone groups of QH-AmDH from *P. denitrificans* (*3*) by using a mediator-assisted continuous-flow column electrolytic spectroelectrochemistry (MCES), which has been developed by our groups for protein $E^{\circ\prime}$ measurements (*13*, *26*). The spectroelectrochemical titration curve showed only one step in the redox reaction of the heme group(s) with isosbestic points, which gave a value for $E^{\circ\prime}$ of the heme group(s). The $E^{\circ\prime}$ value of the quinone moiety was indirectly evaluated from the substrate titration curve of the heme group(s). At that time, however, the number of heme *c* groups was believed to be unity on the basis of the chemical analysis. Therefore, re-evaluation of $E^{\circ\prime}$ is needed.

To date, there are a limited number of reports of $E^{\circ\prime}$ values of quinohemoproteins, namely, ethanol dehydrogenase from *Comamonas testosteroni* containing one PQQ and one heme *c* in the molecule (*27*) and membrane-bound alcohol dehydrogenase from *Acetobacter methanolicus* containing one PQQ and four heme *c* groups in the molecule (*28*). The evaluations of $E^{\circ\prime}$ values were based on a conventional redox titration, but were limited to the heme groups. This may be due to the small absorption coefficients of the quinone groups compared with those of the heme groups and to the spectroscopic overlapping of the quinone and the heme groups. Our group also applied a column electrolytic spectroelectrochemical method for the $E^{\circ\prime}$ determination of PQQ- and four heme-containing alcohol dehydrogenase (*29*). However, the evaluated data did not lead to a general consensus, since the resulting $E^{\circ\prime}$ values of the heme groups were not in accord with those evaluated by a conventional titration method (*28*). Furthermore, the $E^{\circ\prime}$ value of PQQ was evaluated from a small absorption change around the Soret band. Direct electrochemistry of quinohemoproteins (as well as flavohemoproteins) is also very useful from a bioelectrochemical point of view (*30*−*32*). However, the direct electrochemical signal was ascribed to only heme groups if any, and direct electrochemical information concerning organic cofactors has not been obtained.

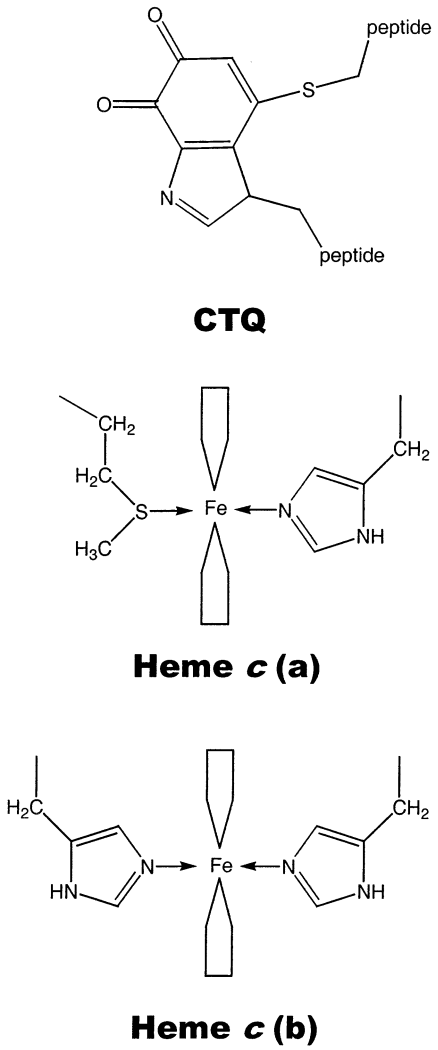

FIGURE 2: Structure of CTQ and schematic features of the axial ligands of the two hemes *c* in QH-AmDH.

In this paper, we attempted to re-evaluate the $E^{\circ\prime}$ values of the two hemes *c* of QH-AmDH by using MCES through a thermodynamic and kinetic analysis. Since native QH-AmDH gives no direct electrochemical signal, the γ subunit was isolated and the $E^{\circ\prime}$ value of CTQ and its pH dependence were determined. These data are used to discuss the intra- and intermolecular electron transfer of QH-AmDH.

EXPERIMENTAL PROCEDURES

Purification and Preparation of QH-AmDH. QH-AmDH from *P. denitrificans* was isolated and purified as described in the literature (*3*, *24*), and the concentration of the reduced protein was determined from the absorbance at 552 nm (ϵ_{552} = 37.2 mM^{-1} cm^{-1}). The fully oxidized and reduced forms of QH-AmDH were prepared by adding $K_3Fe(CN)_6$ and *n*-butylamine or $Na_2S_2O_4$, respectively.

Purification and Preparation of the γ Subunit of QH-AmDH. The γ subunit of QH-AmDH was isolated as follows. A portion of the fully oxidized QH-AmDH was treated with 8 M urea in 100 mM Tris buffer (pH 8.5). The sample was separated by high-performance gel filtration chromatography with a Superdex 200 HR 26/60 column and urea-free 50 mM phosphate buffer containing 150 mM NaCl (pH 7.5). The protein concentration was determined by a weighing method,

in which the sample was desalted by dialysis against pure water (five times) and lyophilized, or a Bradford method (*33*).

Spectroscopy. UV−visible absorption spectroscopy was carried out with a Shimadzu UV-2500(PC)S or Shimadzu UV-1500PC photodiode array spectrophotometer with quartz cells with a light path length of 1 cm at room temperature.

Mediator-Assisted Continuous-Flow Column Electrolytic Spectroelectrochemistry (MCES). This technique is based on the spectroscopic detection of the redox states of proteins equilibrated in a continuous-flow redox buffer regulated by column electrolysis (*26*). Potassium ferricyanide, 2,6-dimethylbenzoquinone, *N*-methylphenazinium methosulfate (PMS), phenazine ethosulfate (PES), 1,4-naphthoquinone, vitamin K_3, and 2-hydroxy-1,4-naphthoquinone [the $E^{\circ\prime}$ values of these compounds at pH 7.0 being 0.443, 0.169, 0.08, 0.055, 0.036, 0.009, and −0.139 V vs SHE, respectively (*34*)] were used as mediators. In this study, a portion of a protein sample (usually 10 μL and on the order of 50 μM) was injected on a mobile phase buffer and mixed with a mixed mediator solution in a two-channel flow injection system. Mobile phase buffers that were used were 0.1 M succinate (pH 6.0), potassium phosphate (pH 7.5), Tris (pH 8.0), D-α-alanine (pH 9.0), or carbonate (pH 10.0) at an ionic strength of 0.3 M with KCl. The mixed mediator solution and the mobile phase buffer were thoroughly degassed with argon and flowed at a rate in the range of 0.35−2.0 mL/min. Other details of the principle, instruments, and methods are described in the literature (*13*, *26*). All potentials in this paper are referred to the standard hydrogen electrode (SHE), unless stated otherwise.

Electrochemistry. Cyclic voltammetry was performed on an HZ-3000 instrument (Hokuto Denko Co.) using an Ag/AgCl/KCl (saturated) reference electrode and a Pt-disk counter electrode. A bare grassy carbon electrode (inside diameter of 3.0 mm, Bioanalytical Systems) as a working electrode was polished with alumina powder (particle size of 0.05 μm) and sonicated in distilled water for ∼15 min. The cell was deaerated by passing argon gas through the electrochemical cell for more than 15 min before the experiments were carried out.

RESULTS

Redox Potentials of Two Hemes c in QH-AmDH. QH-AmDH exhibited reproducible spectral changes depending on the electrode potential (*E*) in MCES at a flow rate of 0.35 mL/min at pH 7.0 (0.1 M potassium phosphate, ionic strength 0.3 M with KCl) in the presence of mixed mediators (Figure 3). The spectral change is characteristic of the redox reaction of heme *c* groups. The absorption spectra obtained at 0.4 and −0.1 V were almost identical with those of the fully oxidized form [prepared by the oxidation with $K_3Fe(CN)_6$] and the fully reduced one (prepared by the reduction with *n*-butylamine or $Na_2S_2O_4$), respectively. During the spectral change, isosbestic points appeared at 342, 411, 440, 510, 538, and 561 nm. Any direct information concerning the redox reaction of CTQ was not obtained spectroscopically. The spectra remained practically unchanged in the potential regions of −0.4 to −0.1 V and of 0.4−0.6 V.

The *E* dependence of the absorbance at 418 nm (A_{418}) depicted in Figure 4 shows only a one-step change. The

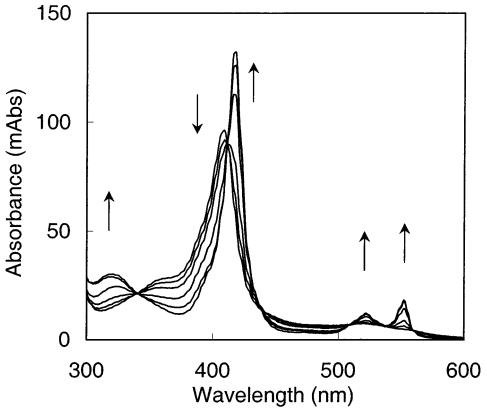

FIGURE 3: Background-corrected absorption spectra of QH-AmDH at 0.397 (fully oxidized), 0.297, 0.222, 0.147, 0.047, and −0.103 V (fully reduced) and pH 7.0. An aliquot of a fully oxidized QH-AmDH sample (50 μM × 10 μL) was injected at each electrode potential into an MCES system with a flow rate of 0.35 mL/min. The following mediators were used: 50 μM potassium ferricyanide, 125 μM 2,6-dimethylbenzoquinone, 20 μM *N*-methylphenazinium methosulfate (PMS), 10 μM phenazine ethosulfate (PES), 10 μM vitamin K_3, and 75 μM 2-hydroxy-1,4-naphthoquinone. The arrows indicate the direction of the spectral changes upon reduction of QH-AmDH.

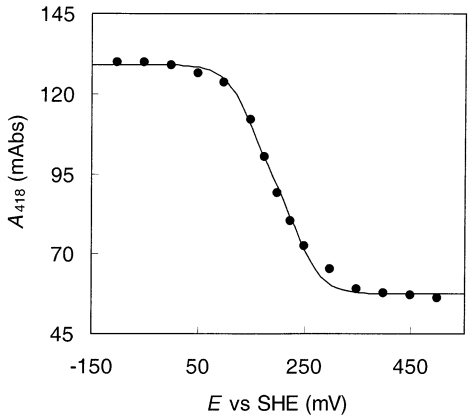

FIGURE 4: Spectroelectrochemical titration curve of QH-AmDH taken by the MCES method under equilibrated conditions, the details of which are given in the legend of Figure 3: (●) experimental data and (−) nonlinear regression curve calculated on the basis of eq 3.

titration curve was practically independent of the direction and width of the potential step and the flow rate at least up to 0.5 mL/min. The results strongly support the idea that the redox reaction between QH-AmDH and the mediators reached equilibrium states under these conditions. All these results are practically identical with those reported in a previous paper (*3*).

Since QH-AmDH has two hemes *c* in the molecule, we hypothesize that the spectral change is assigned to the redox reaction of two hemes *c* alone. Combination of the hypothesis and the one-step sigmoidal characteristics of the titration curve leads to the conclusion that the $E^{\circ\prime}$ value of heme *c*(b) with His as the second axial ligand is close to that of heme *c*(a) with Met as the second axial ligand. However, this conclusion appears to contradict the reported characteristics of hemes *c* with bis-His axial ligands, which have fairly negative $E^{\circ\prime}$ values compared with usual hemes *c* with Met as the second axial ligand (*35*). In addition, combination of the hypothesis and the appearance of the isosbestic points

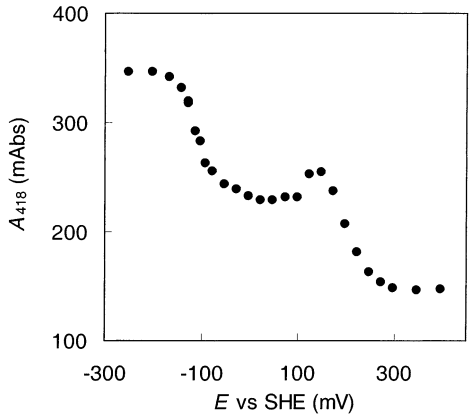

FIGURE 5: Absorbance at 418 nm (A_{418}) of QH-AmDH as a function of the electrode potential (*E*) taken by the MCES method under nonequilibrium high-flow rate conditions at pH 7.0. The fully oxidized species (10 μL, 50 μM) was injected at each *E*. The flow rate of MCES was 2 mL/min, and the following mediators were used: 50 μM potassium ferricyanide, 125 μM 2,6-dimethylbenzoquinone, 10 μM vitamin K_3, and 75 μM 2-hydroxy-1,4-naphthoquinone.

in the spectral change leads to another conclusion that heme *c*(b) is very similar to heme *c*(a) in the spectral property despite the difference in the second axial ligand. Therefore, it is very important and indispensable to confirm the hypothetical assignment of the spectral change in the one-step sigmoidal titration curve.

Kinetic Distinction between Heme c(a) and Heme c(b). For the above purpose, we attempted to distinguish heme *c*(b) from heme *c*(a) by a kinetic analysis. The MCES method is useful for obtaining kinetic information about the electron transfer between proteins and mediators, where the reaction time is controlled by the flow rate (*13*). At increased flow rates, the spectrum of QH-AmDH electrolyzed on the MCES system depended on the flow rate. This means that QH-AmDH was eluted before it reached equilibrium with the mediators. Under such kinetically controlled conditions, the A_{418} versus *E* curve clearly showed two-step characteristics, as shown in Figure 5, where the flow rate was 2.0 mL/min, and PMS and PES were removed from the mixed mediator solution to reduce the rate of electron exchange between QH-AmDH and the mediators. The appearance of the two-step wave reflects the difference in the reduction kinetics of the two hemes *c* (note that the oxidized form of QH-AmDH was injected for each data point in this case). The absorbance of QH-AmDH in Figure 5 was larger than that in Figure 4 despite the same amount of protein being injected, which is true because dilution and diffusion of the protein sample in the column are relatively suppressed at increased flow rates, leading to sharp elution peaks. Other spectral properties were almost identical with those obtained under equilibrium conditions, although the titration curve showed a peak shape in the first step of reduction. The observation of the two-step redox curves strongly supports the hypothetical assignment that the one-step characteristics of the titration curve under equilibrated conditions reflect the sequential redox reaction of the two heme *c* groups.

Evaluation of $E^{o\prime}$ Values of Two Heme c Groups. The Nernst equations of the heme groups (H_L and H_H, L and H denoting the hemes with lower and higher $E^{\circ\prime}$ values, respectively) are given by

$$\frac{[H_{L,ox}]}{[H_{L,red}]} = \exp\left[\frac{F}{RT}(E - E_L^{\circ\prime})\right] \equiv \eta_L \quad (1)$$

$$\frac{[H_{H,ox}]}{[H_{H,red}]} = \exp\left[\frac{F}{RT}(E - E_H^{\circ\prime})\right] \equiv \eta_H \quad (2)$$

where subscripts ox and red denote the oxidized and reduced forms of the heme, respectively. The brackets indicate the concentration of the corresponding species, and *F*, *R*, and *T* have the usual meaning. Here, we assume that two heme *c* groups undergo the redox reaction independently. Since the CTQ-related absorption coefficient would be negligibly small compared with that of two hemes *c*, the relationship between the absorbance (*A*) and *E* can be expressed by

$$A = (\epsilon_{L,ox}[H_{L,ox}] + \epsilon_{L,red}[H_{L,red}] + \epsilon_{H,ox}[H_{H,ox}] + \epsilon_{H,red}[H_{H,red}])l$$

$$= \frac{\eta_H A_1}{\eta_H + 1} + \frac{(\eta_L - \eta_H)A_2}{(\eta_H + 1)(\eta_L + 1)} + \frac{A_3}{\eta_L + 1} \quad (3)$$

with

$$A_1 = (\epsilon_{H,ox} + \epsilon_{L,ox})[P]l \quad (4)$$

$$A_2 = (\epsilon_{H,red} + \epsilon_{L,ox})[P]l \quad (5)$$

$$A_3 = (\epsilon_{H,red} + \epsilon_{L,red})[P]l \quad (6)$$

where $\epsilon_{L,ox}$, $\epsilon_{L,red}$, $\epsilon_{H,ox}$, and $\epsilon_{H,red}$ are the absorption coefficients of the corresponding species, [P] (=$[H_{L,ox}] + [H_{L,red}] = [H_{H,ox}] + [H_{H,red}]$) denotes the total concentration of QH-AmDH, and *l* is the length of the light path ([P]*l* being constant under the experimental conditions). The *A* value reduces to A_1 when $E \gg E_H^{\circ\prime} > E_L^{\circ\prime}$ ($\eta_H > \eta_L \gg 1$) or to A_3 when $E \ll E_L^{\circ\prime} < E_H^{\circ\prime}$ ($\eta_L < \eta_H \ll 1$), and then A_1 and A_3 can be evaluated experimentally from the plateaus of the titration curve in Figure 4. When the close similarity of the spectroscopic property of the two hemes is considered, it can be reasonably assumed that $\epsilon_{L,ox} \approx \epsilon_{H,ox}$ and $\epsilon_{L,red} \approx \epsilon_{H,red}$; that is, $A_2 \approx (A_1 + A_3)/2$. Therefore, eq 3 can be fitted to the titration curve using $E_H^{\circ\prime}$ and $E_L^{\circ\prime}$ (or η_H and η_L) as the adjustable parameters by nonlinear regression analysis. The Nernstian analysis yielded values of 0.235 ± 0.006 and 0.149 ± 0.003 V for $E_H^{\circ\prime}$ and $E_L^{\circ\prime}$, respectively (the deviation being given as the goodness of the fitting). The regression curve can reproduce well the experimental data, as shown by the solid line in Figure 4.

Purification and Spectral Properties of the γ Subunit. The gel chromatographic separation of urea-treated QH-AmDH yielded three major peaks. The molecular mass of the third peak was assessed to be ca. 9 kDa, which is close to the calculated mass of the γ subunit (8.5 kDa) (*19*). Then, it can be concluded that the third peak corresponds to the γ subunit of QH-AmDH. When the γ subunit fraction was reassayed by gel chromatography, the retention time was almost identical with that of the first one. Therefore, it can be concluded that the isolated γ subunit is monomeric even in the absence of urea. The γ subunit oxidized with $K_3Fe(CN)_6$ gave a characteristic broad absorption band centered at 380 nm. This absorption band overlaps with the Soret band

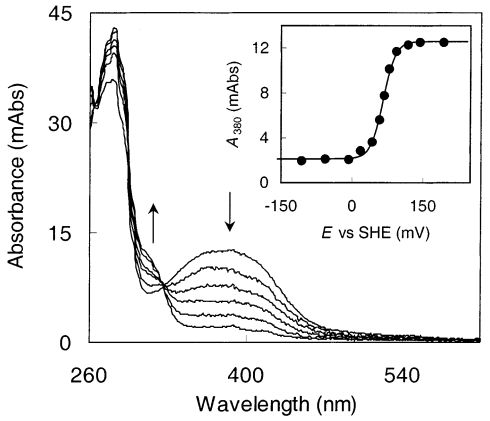

FIGURE 6: Background-corrected absorption spectra of the γ subunit of QH-AmDH at 0.193 (fully oxidized), 0.078, 0.068, 0.058, 0.043, and −0.057 V (fully reduced) at pH 7.0. An aliquot of the γ subunit (50 μM, 10 μL) was injected into an MCES system with a flow rate of 0.35 mL/min at each electrode potential. The following mediators were used: 30 μM *N*-methylphenazinium methosulfate (PMS) and 20 μM phenazine ethosulfate (PES). The arrows indicate the direction of the spectral changes on the reduction of the γ subunit. The inset shows the spectroelectrochemical titration curve of the γ subunit obtained by the MCES method at 380 nm: (●) experimental data and (−) nonlinear regression curve determined on the basis of a one-step two-electron transfer model.

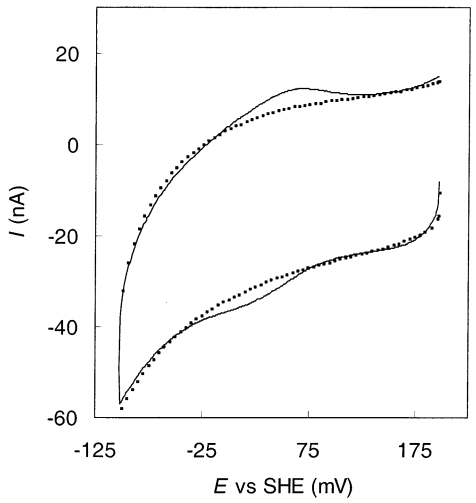

FIGURE 7: Cyclic voltammograms of the γ subunit of QH-AmDH. Solid and broken lines are cyclic voltammograms in the presence and absence of 5.2 μM γ subunit, respectively, at a glassy carbon electrode at a scan rate of 5 mV/s in 0.05 M potassium phosphate (pH 7.0).

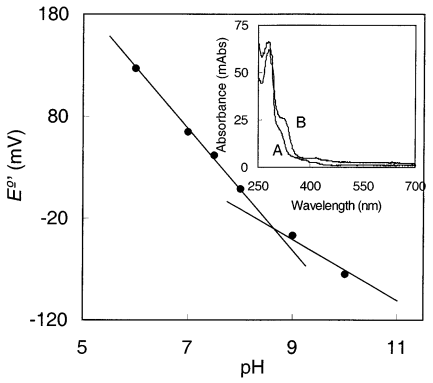

FIGURE 8: $E^{\circ\prime}$ values of CTQ in the isolated γ subunit as a function of pH. The slopes of the two straight lines are −60 and −30 mV/pH unit. Mediators identical to those given in the legend of Figure 6 were used, except at pH 10.0 where 15 μM PMS and 150 μM 1,4-naphthoquinone were used. The inset shows the absorption spectra of the fully reduced form of the isolated γ subunit (3.3 μM) at pH 6.0 (A) and 10.0 (B). The spectra were obtained by the MCES method.

of QH-AmDH. The absorption coefficient was determined to be 7 mM^{-1} cm^{-1} at 380 nm when the peptide contents were evaluated by the weighing method, while a value of 14 mM^{-1} cm^{-1} was obtained from the peptide content data by the Bradford method. The value(s) is significantly smaller than that of the Soret band of QH-AmDH [227 mM^{-1} cm^{-1} at 408 nm for the fully oxidized species (*3*)]. Addition of substoichiometric amounts of $Na_2S_2O_4$ to the γ subunit caused a decrease in the magnitude of the broad band around 380 nm. However, it was difficult to obtain the absorption spectrum of the fully reduced form due to the spectral overlap with $Na_2S_2O_4$. The γ subunit retained dehydrogenase activity for *n*-butylamine with $K_3Fe(CN)_6$ as an electron acceptor, but the activity is very low (10^4 times lower than that of native QH-AmDH). The γ subunit was slightly unstable at room temperature, the lifetime being ∼5 h, as judged from the spectral change.

Electrochemistry of the γ Subunit. Using the MCES method, we have the capacity to obtain background-corrected absorption spectra of proteins in the presence of mediators (*13*, *26*). To determine the absorption spectrum of the fully reduced form, the isolated γ subunit was analyzed by the MCES method at a flow rate of 0.35 mL/min at pH 7.0 in the presence of mixed mediators. The column electrode reduction of the γ subunit caused a decrease in the magnitude of the broad band around 380 nm and an increase in the magnitude of a new shoulder band around 315 nm, giving an isosbestic point at 326 nm, as shown in Figure 6. The spectroelectrochemical titration curve showed a Nernstian response (Figure 6, inset) and was well reproduced on the basis of a one-step two-electron transfer model (*13*, *36*, *37*). The nonlinear regression analysis of the titration curve yielded an $E^{\circ\prime}$ of 0.065 ± 0.002 V at pH 7.0.

The isolated γ subunit gave a pair of cathodic and anodic waves on a cyclic voltammogram at a bare glassy carbon electrode (Figure 7). This redox wave is reasonably assigned to CTQ. The peak separation was ca. 50 mV at a scan rate (υ) of 5 mV/s. However, the peak currents were proportional to υ, and almost independent of the concentration (at least at ≥2 μM), indicating quasi-reversible characteristics due to the adsorbed species of the γ subunit. The midpoint potential was determined to be 0.042 V at pH 7.0.

Figure 8 shows the pH dependence of $E^{\circ\prime}$ of the CTQ cofactor in the isolated γ subunit, $E^{\circ\prime}$ being evaluated by the MCES method. Changes of −60 and −30 mV/pH unit were observed with an inflection at pH 8.6. The results indicate that the two-electron transfer of CTQ is linked to the transfer of two protons at pH <8.6, and of a single proton at pH >8.6. The pH value of the inflection point (8.6) corresponds to a pK_a value of the quinol form of CTQ (*38*), K_a being the acid dissociation constant. A red shift of the shoulder band (longest $\pi-\pi^*$ band) of the quinol form was observed upon deprotonation of the quinol form, as shown in the inset of Figure 8, while the absorption spectrum of the oxidized CTQ remained unchanged in the pH region that was examined (pH 6−10) (data not shown).

DISCUSSION

This study has, for the first time, revealed the absorption spectra of the fully oxidized and reduced CTQ bound to the γ subunit of QH-AmDH. The fully oxidized form gave a characteristic broad absorption band around 380 nm with an absorption coefficient of 7 mM^{-1} cm^{-1} by the weighing method as a peptide content assay (or 14 mM^{-1} cm^{-1} by the Bradford method). The wavelength and the absorption coefficient of the longest $\pi-\pi^*$ band of CTQ are shorter and smaller, respectively, than those of TTQ enzymes [$\sim$450 nm and $\sim$20−25 mM^{-1} cm^{-1}, respectively (*5*, *12*)]. The small increase in the magnitude of the shoulder band of the fully reduced CTQ around 315 nm is also compared with a large increase seen with TTQ enzymes upon reduction (*5*, *12*). These differences in the spectroscopic properties of CTQ from TTQ seem to be due to a decreased level of π-stabilization of tryptophylquinone and its quinol by cross-linking to Cys instead of aromatic Trp, although the π-conjugation in a free state of a TTQ model compound is not so strong (*38*).

The absorption coefficient of CTQ and its change with the redox reaction are very small compared with those of the Soret band of the heme groups. In addition, the absorption band of CTQ partially overlaps with the Soret band. These are the reasons why it was very difficult to extract the information about the redox reaction of CTQ from the spectral change of QH-AmDH. This consideration also indicates that the spectral change of QH-AmDH reflects the redox reaction of the heme *c* groups alone.

The isolated γ subunit gave a direct electrochemical signal of CTQ at a bare glassy carbon electrode. This is very interesting since direct electrochemistry has not yet been realized for quinone cofactors of quinoproteins. Most probably, the small size of the γ subunit is responsible for the successful observation of the direct electron transfer to and/or from the electrode. However, the response was ascribed to the adsorbed species so that the midpoint potential (0.042 V) evaluated from the voltammogram includes the difference in the adsorption energy between the fully oxidized and reduced γ subunit (*39*, *40*). In contrast, the MCES method provided information concerning the soluble species under equilibrated conditions, and the midpoint potential (0.065 V) evaluated by MCES (Figure 6) is more reliable for the $E^{\circ\prime}$ of the CTQ cofactor, in this case, than that of cyclic voltammetry. The latter is slightly more negative than the former, suggesting that the fully reduced γ subunit adsorbs more strongly on the electrode than the fully oxidized one (*39*).

The $E^{\circ\prime}$ value of CTQ evaluated in this work could be somewhat different from that of the native one, because the isolated γ subunit is likely to be less structured than it is in the complete QH-AmDH. However, the $E^{\circ\prime}$ value is close to that of TTQ in MADH from *P. denitrificans* [0.100 V at pH 7.5 (*12*) and 0.130 V at pH 7.5 (*13*)] and that of a TTQ model compound [0.107 V at pH 7.0 (*38*)]. This result seems to be reasonable since both CTQ and TTQ have the same tryptophylquinone skeleton. Therefore, the $E^{\circ\prime}$ value of CTQ evaluated here can be accepted as that of the native one to a first approximation.

The two- and single-proton transfer linked to the two-electron transfer of CTQ and the pK_a (8.6) of one of the phenolic OH groups of the quinol form are compared with those of TTQ. In MADH, the single-proton transfer is linked to the two-electron transfer in the pH range of 6.2−8.3 (*41*), indicating that the pK_a value of the TTQ quinol in MADH is less than 6. In a TTQ model compound, a two-proton transfer occurs at pH <10 and the pK_a of the TTQ quinol is 10.1 (*38*). The difference may be explained by the difference in the environments of the quinone cofactors; the γ subunit could be disordered in part, and CTQ is more solvent accessible than TTQ in MADH.

There was no evidence for the presence of the semiquinone form of CTQ in the redox titration or in the spectral change. This result suggests that the one-electron redox potential of CTQ and the semiquinone couple is more negative by $\sim$100 mV than that of the semiquinone and the fully reduced CTQ couple for the isolated γ subunit (*40*). In contrast, for QH-AmDH an ESR signal of the semiquinone has been observed upon partial reduction (*3*), indicating thermodynamic stabilization of the CTQ semiquinone in the enzyme. Destabilization of the semiquinone in the isolated γ subunit would be due to an increased solvent accessibility of CTQ.

The γ subunit exhibited dehydrogenase activity for *n*-butylamine with $K_3Fe(CN)_6$ as an electron acceptor, although the activity was very low. Such behavior can be expected, since all the other quinone cofactors exhibit similar catalytic activity for oxidative deamination of amines (such as benzylamine) in the free state (*38*, *42*−*45*). However, we did not carry out further kinetic experiments (for example, on substrate or cosubstrate specificity), since the γ subunit could be in part denatured.

This study also has clearly revealed that the one-step profile of the spectroelectrochemical titration curve (Figure 4) can be ascribed to the redox reaction of the two hemes *c* in QH-AmDH. The appearance of the isosbestic points in the titration curve (Figure 3) indicates that the spectral properties of heme *c*(a) and heme *c*(b) are very similar despite the difference in the second axial ligand. On the basis of these considerations, the titration curve was successfully analyzed using a model in which two heme *c* groups undergo the redox reaction independently (independent model), yielding $E_H^{\circ\prime}$ and $E_L^{\circ\prime}$. An alternative model involving an interactive two-step one-electron transfer, where $E^{\circ\prime}$ of one heme depends on the redox state of the other heme (interactive model), also was applied to the analysis of the titration curve. The major difference in the interpretation of titration curves between the two models appears only in the case when the two $E^{\circ\prime}$ values become similar or are reversed with respect to each other. The cooperative multistep redox reactions in the interactive model occur in proton transfer-coupled electron transfers (as in the case of quinones) (*13*, *37*, *40*, *46*) or conformational change-coupled electron transfers (*47*, *48*). In our case, the result analyzed by the interactive model was identical to that obtained with the independent model (data not shown). Therefore, we cannot conclude from the thermodynamic analysis whether the two heme *c* groups interact with each other. However, since the distance between two iron atoms of hemes *c*(a) and *c*(b) is $\sim$16 Å (*19*), the interaction would not be so strong, if it existed at all.

The other interesting feature is that the two hemes *c* were well distinguished from each other with respect to the reduction kinetics of QH-AmDH with the mediators. The A_{418} versus *E* profile under nonequilibrium conditions (Figure

5) gave apparent midpoint potentials of the first and second one-electron reductions of approximately 0.2 and −0.1 V, respectively. The former is relatively close to the $E_H^{\circ\prime}$ value (0.235 V) evaluated by MCES under equilibrated conditions, but the latter is more negative than $E_L^{\circ\prime}$ (0.149 V). This suggests that the reduction of the heme *c* of $E_H^{\circ\prime}$ with mediators is fast compared with that of the other heme. Most probably, heme *c* of $E_H^{\circ\prime}$ is more solvent-accessible than the other. When the crystallographic structure of QH-AmDH is considered (*19*), heme *c* of $E_H^{\circ\prime}$ is reasonably assigned to heme *c*(a) with Met as the second axial ligand, and the other is assigned to heme *c*(b) with His as the second axial ligand. This assignment is consistent with the nature of the iron ligation (*35*).

The following question arises here about the A_{418} versus *E* profile under the kinetic conditions: why does the first one-electron reduction step exhibit a peak shape (Figure 5)? The reason is not clear, but the electrode potential where the peak shape appeared (ca. 0.14 V) is close to $E^{\circ\prime}$ of 2,6-dimethylbenzoquinone (0.169 V), one of the mediators that was used. This mediator is susceptible to adsorption on the carbon fiber electrode surface in the column electrode, and the adsorption coefficients of the oxidized and reduced forms must be different. In addition, the rate of electron transfer from the mediator to QH-AmDH would be affected by the soluble or adsorbed states of mediators. This might be one of the causes of the appearance of the peak in the titration curve. Note that such an adsorption effect (or kinetic effect) does not disturb the titration curve under equilibrated conditions.

The $E^{\circ\prime}$ value of heme *c*(a) is close to those of horse heart cytochrome *c* [0.255 V (*49*)] and cytochrome c_{550} [0.243 V (*24*)], both of which have Met as the second axial ligand. On the other hand, bis-His axial hemes *c* occur in cytochrome c_3 from *Desulfovibrio vulgaris* (*22*) and in tetraheme *c*-type cytochrome from *Paracoccus denitrificans* (*50*). The $E^{\circ\prime}$ values of these hemes *c*, which are in the range of −0.4 to 0 V, are more negative than those of usual cytochromes *c* (*34*, *35*, *50*−*52*). It has also been reported that the second axial ligand replacement of His with Met in one of the four hemes *c* in cytochrome c_3 causes a large positive shift in $E^{\circ\prime}$ by at least 0.2 V (*53*). Further, the $E^{\circ\prime}$ values of two hemes *c* in diheme cytochrome *c* peroxidase have been reported to be 0.320 and −0.330 V, the second axial ligands of which are Met and His, respectively (*23*). Heme *c*(b) of QH-AmDH is only 0.086 V more negative in $E^{\circ\prime}$ than heme *c*(a), and considerably more positive than the bis-His axial hemes *c* reported so far. This is a very interesting feature, and such an unusual thermodynamic property might be due to the low solvent accessibility of heme *c*(b) in QH-AmDH.

The crystal structure of QH-AmDH (*19*) suggests that the electron transfer pathway from CTQ to heme *c*(a) occurs via heme *c*(b) (Figure 1). The thermodynamic study presented here supports this prediction. The $E^{\circ\prime}$ values of these redox centers are located in this case from the negative to the positive direction.

Cytochrome c_{550}, the physiological electron acceptor of QH-AmDH in *P. denitrificans*, has an $E^{\circ\prime}$ of 0.243 V (pH 7.5) (*24*), which is slightly more positive than that of heme *c*(a). Heme *c*(a) is more solvent accessible and is located in a more hydrophilic environment than heme *c*(b) (*19*). These properties of heme *c*(a) seem to make it possible for it to function as a site donating an electron to the hydrophilic cytochrome c_{550}. However, it is very important to note that very fast electron transfer ($k_{cat} = 4.7\ s^{-1}$, $K_M \leq 0.1\ \mu M$, $k_{cat}/K_M \geq 4.7 \times 10^7\ M^{-1}\ s^{-1}$) occurs from heme *c*(a) to cytochrome c_{550} despite the relatively small difference in $E^{\circ\prime}$ (*54*). This may be due to the short distance in the two redox centers and low reorganization energy (*55*). The proposed interprotein electron transfer in QH-AmDH is compared with that of MADH/amicyanin, where hydrophobic interactions play an important role (*15*) and the difference in $E^{\circ\prime}$ is as large as 0.1 V, although ionic interactions also function cooperatively (*16*−*18*). For a more detailed understanding of these intra- and interprotein electron transfer reactions, structural analysis of the QH-AmDH−cytochrome c_{550} complex and kinetic and thermodynamic analyses coupled with site-directed mutagenesis will be required.

REFERENCES

1. Anthony, C. (1990) *Antonie van Leeuwenhoek 56*, 13−23.
2. Husain, M., and Davidson, V. L. (1987) *J. Bacteriol. 169*, 1712−1717.
3. Takagi, K., Torimura, M., Kawaguchi, K., Kano, K., and Ikeda, T. (1999) *Biochemistry 38*, 6935−6942.
4. Iwaki, M., Yagi, T., Horiike, K., Saeki, Y., Ushijima, T., and Nozaki, M. (1983) *Arch. Biochem. Biophys. 220*, 253−262.
5. Govindaraj, S., Eisenstein, E., Jones, L. H., Sanders-Leohr, J., Chistoserdov, A. Y., Davidson, V. L., and Edwards, S. L. (1994) *J. Bacteriol. 176*, 2922−2929.
6. Shinagawa, E., Matsushita, K., Nakashima, K., Adachi, O., and Ameyama, M. (1998) *Agric. Biol. Chem. 52*, 2255−2263.
7. Adachi, O., Kubota, T., Hacisalihoglu, A., Toyama, H., Shinagawa, E., Duine, J. A., and Matsushita, K. (1998) *Biosci., Biotechnol., Biochem. 62*, 469−478.
8. McIntire, W. S., Wemmer, D. E., Chistoserdov, A., and Lidstrom, M. E. (1991) *Science 252*, 817−824.
9. Husain, M., and Davidson, V. L. (1985) *J. Biol. Chem. 260*, 14626−14629.
10. Chistoserdov, A. Y., Boyd, J., Mathews, F. S., and Lidstrom, M. E. (1992) *Biochem. Biophys. Res. Commun. 184*, 1181−1189.
11. Davidson, V. L., and Jones, L. H. (1991) *Anal. Chim. Acta 249*, 235−240.
12. Husain, M., and Davidson, V. L. (1987) *Biochemistry 26*, 4139−4143.
13. Sato, A., Torimura, M., Takagi, K., Kano, K., and Ikeda, T. (2000) *Anal. Chem. 72*, 150−155.
14. Burrows, A. L., Hill, H. A., Leese, T. A., Mcintire, W. S., Nakayama, H., and Sanghera, G. S. (1991) *Eur. J. Biochem. 199*, 73−78.
15. Chen, L., Durley, R., Poliks, J. B., Hamada, K., Chen, Z., Mathews, F. S., Davidson, V. L., Satow, Y., Huizinga, E., Vellieux, F. M. D., and Hol, W. G. J. (1992) *Biochemistry 31*, 4959−4964.
16. Davidson, V. L., Johns, L. H., Graichen, M. E., Mathews, F. S., and Hosler, J. P. (1997) *Biochemistry 36*, 12733−12738.
17. Zhu, Z., Curane, L. M., Chen, Z., Durley, R. C. E., Mathews, F. S., and Davidson, V. L. (1998) *Biochemistry 37*, 17128−17136.
18. Zhu, Z., Johns, L. H., Graichen, M. E., and Davidson, V. L. (2000) *Biochemistry 39*, 8830−8836.
19. Datta, S., Mori, Y., Takagi, K., Kawaguchi, K., Chen, Z., Okajima, T., Kuroda, S., Ikeda, T., Kano, K., Tanizawa, K., and Mathews, F. S. (2001) *Proc. Natl. Acad. Sci. U.S.A. 98*, 14268−14273.
20. Satoh, A., Kim, J. K., Miyahara, I., Devreese, B., Vandenberghe, I., Hacisalihoglu, A., Okajima, T., Kuroda, S., Adachi, O., Duine, J. A., Van Beeumen, J., Tanizawa, K., and Hirotsu, K. (2002) *J. Biol. Chem. 277*, 2830−2834.
21. Timkovich, R., and Dickerson, R. E. (1975) *J. Biol. Chem. 251*, 4033−4046.
22. Higuchi, Y., Bando, S., Kusunoki, M., Matsuura, Y., Yasuoka, N., Kakudo, M., Yamanaka, T., Yagi, T., and Inokuchi, H. (1981) *J. Biochem. 89*, 1659−1662.
23. Fülöp, V., Ridout, C. J., Greenwood, C., and Hajdu, J. (1995) *Structure 3*, 1225−1233.

24. Takagi, K., Yamamoto, K., Kano, K., and Ikeda, T. (2001) *Eur. J. Biochem. 268*, 470−476.
25. Klinman, J. P. (2001) *Proc. Natl. Acad. Sci. U.S.A. 98*, 14766−14768.
26. Torimura, M., Mochizuki, M., Kano, K., Ikeda, T., and Ueda, T. (1998) *Anal. Chem. 70*, 4690−4695.
27. Dejong, G. A. H., Caldeira, J., Sun, J., Jongejan, J. A., Devries, S., Loehr, T. M., Moura, I., Moura, J. J. G., and Duine, J. A. (1995) *Biochemistry 34*, 9451−9458.
28. Frébortova, J., Matsushita, K., Arata, H., and Adachi, O. (1998) *Biochim. Biophys. Acta 1363*, 24−34.
29. Torimura, M., Kano, K., Ikeda, T., and Ueda, T. (1997) *Chem. Lett. 6*, 525−526.
30. Ikeda, T. (1997) in *Frontiers in Biosensorics I, Fundamental Aspects* (Scheller, F. W., Schubert, F., and Fedrowitz, J., Eds.) pp 243−266, Birkhäuser Verlag, Basel, Switzerland.
31. Ikeda, T., Miyaoka, S., and Miki, K. (1993) *J. Electroanal. Chem. 352*, 267−278.
32. Lindgren, A., Larsson, T., Ruzgas, T., and Gorton, L. (2000) *J. Electroanal. Chem. 49*, 105−113.
33. Bradford, M. M. (1976) *Anal. Biochem. 72*, 248−254.
34. Kano, K. (2002) *Rev. Polarogr. 48*, 29−46.
35. Mathews, F. S. (1985) *Prog. Biophys. Mol. Biol. 45*, 1−56.
36. Torimura, M., Mochizuki, M., Kenji, K., Ikeda, T., and Ueda, T. (1998) *J. Electroanal. Chem. 451*, 229−235.
37. Sato, A., Takagi, K., Kano, K., Kato, N., Duine, J. A., and Ikeda, T. (2001) *Biochem. J. 357*, 893−898.
38. Itoh, S., Ogino, M., Haranou, S., Terasaka, T., Ando, T., Komatsu, M., Ohshiro, Y., Fukuzumi, S., Kano, K., Takagi, K., and Ikeda, T. (1995) *J. Am. Chem. Soc. 117*, 1485−1493.
39. Bard, A. J., and Faulkner, L. R. (2001) *Electrochemical Methods: Fundamentals and Applications*, 2nd ed., pp 590−593, Wiley, New York.
40. Kano, K., and Uno, B. (1993) *Anal. Chem. 65*, 1088−1093.
41. Zhu, Z., and Davidson, V. L. (1998) *J. Biol. Chem. 273*, 14254−14260.
42. Itoh, S., Takada, N., Haranou, S., Ando, T., Komatsu, M., Ohshiro, Y., and Fukuzumi, S. (1996) *J. Org. Chem. 61*, 8967−8974.
43. Mure, M., and Klinman, J. P. (1995) *J. Am. Chem. Soc. 117*, 8698−8706.
44. Kano, K., Nakagawa, M., Takagi, K., and Ikeda, T. (1997) *J. Chem. Soc., Perkin Trans. 2*, 1111−1119.
45. Akagawa, M., and Suyama, K. (2001) *Biochem. Biophys. Res. Commun. 281*, 193−199.
46. Wipf, D. O., Wehmeyer, K. R., and Wightman, R. M. (1986) *J. Org. Chem. 51*, 4760−4764.
47. Pierce, D. T., and Geiger, W. E. (1989) *J. Am. Chem. Soc. 111*, 7636−7638.
48. Kano, K., Sugimoto, T., Misaki, Y., Enoki, T., Hatakeyama, H., Oka, H., Hosotani, Y., and Yoshida, Z. (1994) *J. Phys. Chem. 98*, 252−258.
49. Eddowes, M. J., and Hill, H. A. O. (1979) *J. Am. Chem. Soc. 101*, 4461−4464.
50. Roldán, M. D., Sears, H. J., Cheesman, M. R., Ferguson, S. J., Thomson, A. J., Berks, B. C., and Richardson, D. J. (1998) *J. Biol. Chem. 273*, 28785−28790.
51. Moore, G. R., and Pettigrew, G. W. (1990) *Cytochromes c: Evolutionary, Structural and Physicochemical Aspects*, Springer-Verlag, Berlin.
52. Sokol, W. F., Evans, D. H., Niki, K., and Yagi, T. (1980) *J. Electroanal. Chem. 108*, 107−115.
53. Mus-Veteau, I., Dolla, A., Guerlesquin, F., Payan, F., Czjzek, M., Haser, R., Bianco, P., Haladjian, J., Rapp-Giles, B. J., and Wall, J. D. (1992) *J. Biol. Chem. 267*, 16851−16858.
54. Fujieda, N., Mori, M., Kano, K., and Ikeda, T. (2000) *Biochim. Biophys. Acta* (in press).
55. Davidson, V. L. (2000) *Acc. Chem. Res. 33*, 87−93.

BI026387V